(NMR) analysis, using the *tris*[3-(trifluoromethylhydroxymethylene)-(+)camphorato]europium(III) complex. The compound was hydrolyzed to the corresponding acid and then the optical purity was enhanced up to 97% ee by cocrystallization with commercially available *R*-PEA. The optical purity was checked by NMR and circular dichroism spectra: $[\alpha]_D^{25} = -63.2$ (C = 1.01 g/liter tetrahydrofuran).
5. The isotherms were measured from $A = 100$ to 5 Å^2 per molecule.
6. The GIXD measurements were conducted on a liquid surface diffractometer at the undulator beamline BW1 at HASYLAB, Deutsches Elektronen-Synchrotron (DESY). The synchrotron radiation beam was monochromated to a wavelength of 1.339 Å. The incident angle was adjusted to $\alpha_f = 0.85\alpha_c$, where $\alpha_c \approx 0.14°$. A detailed explanation of the method and experimental setup are given in (*7*) and (*8*), respectively. The amphiphile *R*-C_{15}-MA was spread at room temperature in a Langmuir trough and then cooled to 5°C.
7. J. Als-Nielsen *et al*., *Phys. Rep.* **246**, 251 (1994).
8. J. Majewski, *Chem. Eur. J.* **1**, 304 (1995).
9. We implied, although we have not proven, that no significant changes occurred on deposition of the films on a solid support. The AFM measurements were performed with Nanoscope III FM (Digital Instruments, Goleta, CA) at ambient temperature with a commercial silicon nitride tip, attached to a cantilever with a spring constant of 0.38 N/m.
10. Film depositions were done on a NIMA trough (NIMA Technology, Coventry, UK) at 20°C and at a surface pressure of ~40 mN/m. Film was transferred onto mica at a constant speed of 10 mm/min.
11. For the silicon nitride tip used in the AFM studies, the lateral friction coefficient is qualitatively proportional to the hydrophilicity of the surface. A detailed analysis of different factors influencing the lateral friction for self-assembled monolayers on mica is given in Y. Liu *et al*. [*Langmuir* **12**, 1235 (1996)].
12. Crystallographic measurements were performed on a four-circle Rigaku single-crystal diffractometer with Cu K_α radiation from a 18-kW rotating anode generator. The structure was solved and refined with the use of SHELXL-91 software. The coordinates have been submitted to the Cambridge Crystallographic Database.
13. Subtraction of a 25 Å thickness of the crystalline bilayer as in the 3D structure from the 38(4) Å trilayer thickness obtained by AFM leaves 13(4) Å, which is compatible within a standard deviation with the 16(2) Å monolayer thickness.
14. Comparison of the observed and calculated Bragg rods (the latter obtained by x-ray structure factor computations) showed that the alkyl chains on the top level of the trilayer are disordered and there is no ordered binding of PEA from the subphase.
15. Beam damage had in fact occurred, but we lacked the quantitative data to introduce a proper correction.
16. S. P. Zingg, E. M. Arnett, A. T. McPhail, A. A. Bothner-By, W. R. Gilkerson, *J. Am. Chem. Soc.* **110**, 1565 (1988).
17. H. L. Diego, *Acta Chem. Scand.* **48**, 306 (1994).
18. In the complex (*R*-MA, *R*-PEA) the phenyl rings within a layer are uniformly tilted in a manner compatible with close packing of the hydrocarbon chains; in the (*R*-MA, *S*-PEA) salt the phenyl rings are not uniformly tilted.
19. We thank S. Matlis for performing the AFM measurements. Supported by the Minerva Foundation, the German Israeli Foundation (GIF), the Danish Foundation for Natural Sciences, and HASYLAB, DESY, Hamburg, Germany (beam time).

15 July 1996; accepted 8 October 1996

Design of Nonionic Surfactants for Supercritical Carbon Dioxide

J. B. McClain, D. E. Betts, D. A. Canelas, E. T. Samulski, J. M. DeSimone,* J. D. Londono, H. D. Cochran, G. D. Wignall,* D. Chillura-Martino, R. Triolo

Interfacially active block copolymer amphiphiles have been synthesized and their self-assembly into micelles in supercritical carbon dioxide (CO_2) has been demonstrated with small-angle neutron scattering (SANS). These materials establish the design criteria for molecularly engineered surfactants that can stabilize and disperse otherwise insoluble matter into a CO_2 continuous phase. Polystyrene-*b*-poly(1,1-dihydroperfluorooctyl acrylate) copolymers self-assembled into polydisperse core-shell–type micelles as a result of the disparate solubility characteristics of the different block segments in CO_2. These nonionic surfactants for CO_2 were shown by SANS to be capable of emulsifying up to 20 percent by weight of a CO_2-insoluble hydrocarbon into CO_2. This result demonstrates the efficacy of surfactant-modified CO_2 in reducing the large volumes of organic and halogenated solvent waste streams released into our environment by solvent-intensive manufacturing and process industries.

More than 30 billion pounds of organic and halogenated solvents are used worldwide each year as process aids, cleaning agents, and dispersants (*1*), and solvent-intensive industries are considering alternatives that can reduce or eliminate the negative impact that solvent emissions can have on the environment. Because of its low cost, wide availability, and environmentally and chemically benign nature (*2, 3*), CO_2 is an attractive solvent alternative for a wide variety of chemical and industrial processes. Although CO_2, in both its liquid and supercritical (sc) states, readily dissolves many small molecules (*4*), it is a very poor solvent—at easily accessible conditions (temperature <100°C and pressure <300 bar)—for many substances, and commercial applications of pure CO_2 as a solvent have been infrequent. Materials that have disappointingly low solubilities in pure CO_2 include most polymers [except amorphous or low-melting fluoropolymers and silicones (*2, 4, 5*)], waxes, heavy oils, machine-cutting fluids, solder fluxes, photoresists, proteins, salts, and metal oxides. The design and characterization of surfactants that enhance the solubilizing properties of CO_2 is therefore crucial for its widespread application.

Block and graft copolymers composed of chain segments with dissimilar solubility characteristics self-assemble into well-defined structures when placed in a medium that is a good solvent for one of the segments (the lyophilic segment) and a poor solvent for the other segment (the lyophobic segment) (*6–9*). These nonionic surfactants are typified by micelles or more complex aggregates in which the lyophobic segments form a core surrounded by a shell of the highly solvated lyophilic segments that extend into the continuous phase (*6*). The core regions of such micelles are technologically useful, as they are capable of emulsifying otherwise insoluble materials into a microphase-separated environment within a preferred continuous solvent phase (*9*). Here, we report the direct structural characterization by SANS of well-defined, spherical micelles resulting from a series of molecularly engineered block copolymer surfactants in scCO_2. Our results also demonstrate the efficacy of these surfactants in emulsifying insoluble solutes into CO_2. This development may ultimately enable surfactant-modified CO_2 to be used as a replacement for conventional solvent systems currently used in manufacturing and service industries, such as precision cleaning (metal finishing, microelectronics, optics, or electroplating), medical device fabrication, and dry (garment) cleaning, as well as in the chemical manufacturing and coating industries.

Several laboratories have demonstrated progress in the micellization of aqueous and polar materials in many dense sc fluids including alkanes, chlorofluorocarbons, hydrofluorocarbons, and CO_2 (*10–15*). However, success in designing generic surfactants for CO_2 has been hindered by the challenge of identifying lyophilic segments for CO_2. A promising lead for the design of highly effective surfactants for CO_2 arose out of two related discoveries: (i) that CO_2 is thermodynamically a good solvent for fluorinated acrylate polymers [positive second virial coefficient (*13, 16*)], and (ii) that these same polymers could be synthesized

J. B. McClain, D. E. Betts, D. A. Canelas, E. T. Samulski, J. M. DeSimone, Department of Chemistry, University of North Carolina, CB 3290, Venable and Kenan Laboratories, Chapel Hill, NC 27599, USA.
J. D. Londono, H. D. Cochran, G. D. Wignall, Oak Ridge National Laboratory, Oak Ridge, TN 37831, USA.
D. Chillura-Martino and R. Triolo, Departimento di Chimica Fisica, University of Palermo, 90123 Palermo, Italy.
*To whom correspondence should be addressed.

under homogeneous conditions in CO_2 (*17*). Therefore, the fluorinated acrylate segment can be considered as a vehicle to bring insoluble components into CO_2. Recent evidence has shown that fluoroacrylate polymers could be used to bring hydrated, water-soluble polyethylene glycol segments into CO_2 (*10*).

The block copolymers that we have molecularly engineered to be interfacially active in CO_2 are composed of a CO_2-insoluble polystyrene (PS) segment and a CO_2-soluble poly(1,1-dihydroperfluorooctyl acrylate) (PFOA) segment. Because of these solubility differences in CO_2, such block copolymers are predisposed to self-assemble spontaneously into micellular structures in CO_2. We synthesized PS-*b*-PFOA diblock copolymers (Fig. 1) with the "iniferter" technique developed by Otsu (*18*–*20*). We first synthesized the lyophobic PS segment of the surfactant by using tetraethylthiuram disulfide as the initiator. We determined the functionality of the telechelic PS segment by using ultraviolet-visible spectroscopy, and the number-average molecular weight ($\langle M_n \rangle$) was determined from gel permeation chromatography. This functionalized PS segment was then used as a macroinitiator in the photopolymerization of the second monomer, FOA, to form the second lyophilic segment of the diblock copolymer (for simplicity, we will henceforth refer to the block copolymers by listing $\langle M_n \rangle$ for each block, $\langle M_n \rangle_{styrene}$-*b*-$\langle M_n \rangle_{FOA}$).

During the past two decades, SANS has emerged as a powerful technique for studying the self-assembly of amphiphiles in aqueous media (*21*). Experiments to determine the characteristics of PS-*b*-PFOA micelles in $scCO_2$ were performed on the W. C. Koehler 30-m SANS facility at the Oak Ridge National Laboratory (*22*). The neutron wavelength λ was 4.75 Å ($\Delta\lambda/\lambda \approx 5\%$), and the sample detector distance ranged from 6.3 to 10 m, resulting in a range of momentum transfer $0.006 < Q = 4\pi\lambda^{-1} \sin \Theta < 0.1$ Å^{-1}, where 2Θ is the angle of scatter. Instrumental procedures and calibration as well as the procedure for SANS measurements from $scCO_2$ systems have been described (*23*–*27*).

Neutron scattering curves (Fig. 2) from PS-*b*-PFOA in CO_2 were fitted to a spherical "core plus shell" model based on a solid PS core and a uniform-thickness shell containing PFOA chains swollen by CO_2 solvent molecules. Parameters of the model include the aggregation number N_{agg} (the number of block copolymer units forming each micelle), the number of CO_2 molecules N_{CO_2} (that swell the PFOA corona per FOA unit), and the polydispersity parameter $\mathcal{Z}$ (related to the variance of the Schultz distribution of the particle sizes: increasing polydispersity with decreasing $\mathcal{Z}$). The radius of the core (R_{core}) and of the total particle (R_{total}) can be easily derived from these parameters. If we assume no orientational correlations, the coherent differential cross section, $d\Sigma(Q)/d\Omega$, for such a model is given by

$$d\Sigma(Q)/d\Omega = N_p\{\langle F(Q)\rangle^2 + \langle F(Q)\rangle^2[S(Q) - 1]\} + B \quad (1)$$

(*28*), where N_p is the number density of particles, $S(Q)$ is the structure function arising from interparticle scattering, B is the background, and $F(Q)$ is the scattering amplitude of the spherical particle.

Table 1. Characterization of PS-*b*-PFOA micelles in CO_2 (65°C, 340 bar, $\rho = 0.842$ g cm^{-3}) as a function of block lengths.

Surfactant $\langle M_n \rangle_{styrene}$-*b*-$\langle M_n \rangle_{FOA}$	N_{agg}	R_{core} (Å)	R_{total} (Å)	N_{CO_2}	Z_{core}
3.7^k-*b*-16.6^k	7	27	85	40	10
3.7^k-*b*-39.8^k	7	27	89	16	8
3.7^k-*b*-61.2^k	6	26	100	17	8
4.5^k-*b*-24.5^k	8	30	75	16	3
6.6^k-*b*-34.9^k	6	34	77	11	3

A series of PS-*b*-PFOA surfactants having differing lyophilic PFOA segment lengths and lyophobic PS segment lengths were dissolved in CO_2 at 65°C and 340 bar (density $\rho = 0.842$ g cm^{-3}) and characterized by SANS (Table 1). If we rely on calibrated SANS curves, the fit of the scattering results to the core-shell model indicates that the block copolymers self-assemble into spherical core-shell structures (see Fig. 2). A systematic increase of the PFOA block length (the first three entries in Table 1) results in a variation of only the "shell-dependent" properties: an increase in R_{total} and a decrease in the swelling of the corona, evident in N_{CO_2}. The "core-dependent" properties, R_{core} and N_{agg}, remain essentially constant for surfactants of constant PS length. Control of the core-dependent properties is evident in the smooth increases in R_{core} with increasing PS segment length. The behavior of PS-*b*-PFOA surfactants in CO_2 follows the expected scaling laws of micelles composed of block copolymers with variable segment lengths in traditional solvents (*29*, *30*).

The solvent strength of $scCO_2$ is easily tunable with changes in the system density (directly related to temperature and pressure) (*2*, *13*, *16*, *31*). Thus, the association

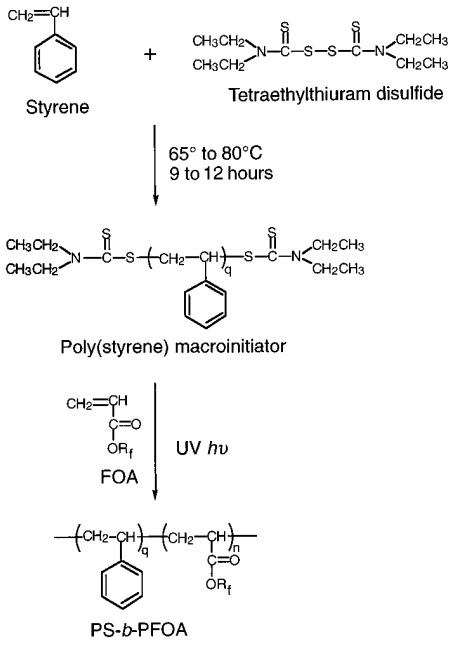

Fig. 1. PS-*b*-PFOA synthesis and structure (*18*). $R_f = CH_2(CF_2)_6CF_3$ and contains ~25% CF_3 branches per molecule.

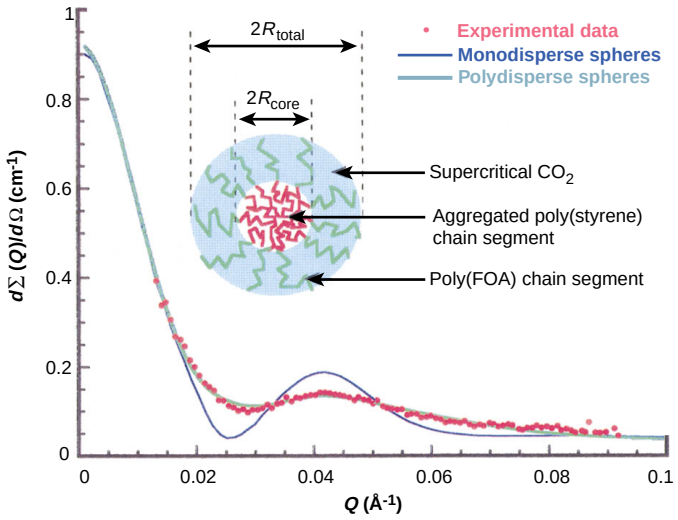

Fig. 2. Plot of $d\Sigma(Q)/d\Omega$ versus Q for 3.7^k-*b*-16.7^k PS-*b*-PFOA in $scCO_2$ (65°C, 340 bar) with fitting to a monodisperse and polydisperse core-shell model.

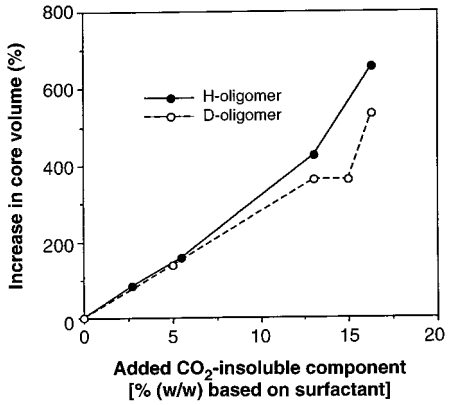

Fig. 3. The swelling of 3.7^k-*b*-39.8^k surfactant micelles in CO_2 (65°C, 340 bar, $\rho = 0.842$ g cm^{-3}) with PS oligomers. Surfactant concentration = 4% (w/v).

of amphiphiles in CO_2 should be strongly dependent on the CO_2 density because of changes in polymer solubility as a function of solvent quality. As the density of CO_2 is increased (*32*), the solvation of both segments becomes greater, which decreases aggregation and creates more dynamic micelles. Thus, we anticipate the existence of a critical micelle density, analogous to a critical micelle concentration, to describe the phenomenon of unimer-to-aggregate transitions for amphiphilic materials in sc fluids with changing solvent (quality) density. Table 2 shows the effect of two experimental conditions—65°C, 340 bar, $\rho = 0.842$ g cm^{-3} and 40°C, 340 bar, $\rho = 0.934$ g cm^{-3} (*31*)—on the association of PS-*b*-PFOA surfactants. With increasing solvent strength (density), smaller and more polydisperse micelles are evident, especially for surfactants with a higher PS/PFOA ratio. When the PFOA segment length is increased to ~135 repeat units, the micelles are essentially unaffected by CO_2 density over this range of conditions.

We demonstrated the ability of a PS-*b*-PFOA micellar solution in CO_2 to emulsify CO_2-insoluble materials by adding model CO_2-insoluble hydrocarbon oligomers (500 g per mole of oligomers of both deuterated and hydrogenated PS, referred to as D-oligomer and H-oligomer, respectively) to the system and monitoring by SANS (*33*). We used both H- and D-oligomer samples to take advantage of different neutron scattering contrasts and to quantify the fraction of oligomer inside the micelle core versus oligomer free in solution or stabilized by free surfactant (*25*). SANS characterization of micelles of PS-*b*-PFOA surfactants in CO_2 (65°C, 340 bar, $\rho = 0.842$ g cm^{-3}) with added H-oligomer and D-oligomer display stabilization of >99% of the added oligomer into the core of the micelle. The micellar core volume increases with added H-oligomer and D-oligomer as a function of oligomer concentration for the 3.7^k-*b*-39.8^k surfactant (*20*) (Fig. 3). By a comparison of the unswollen surfactant micelles with the swollen system containing added oligomer in Table 3, we see an approximately eightfold increase in the volume of the micelle core with the addition of up to 20% (w/w) oligomer.

The density of CO_2, over the same range studied for unswollen aggregates, seems to have little effect on the structure of oligomer-swollen micelles (Table 3). Highly swollen systems were observed for three different surfactants at CO_2 densities ranging from 0.842 to 0.934 g cm^{-3} with less than 5% change in the dimensions or characteristics of the micelles. This is very different from the association behavior of similar unswollen surfactant micelles. In the oligomer-swollen system, the surfactant molecules are forced to an interface between insoluble PS oligomer and CO_2. This effect results in diminished changes in the overall structural dimensions with solvent strength so long as CO_2 remains a good solvent for the PFOA shell segments. Earlier work has shown that PFOA is in a thermodynamically favorable solvent at both densities (*16*) and therefore retains its propensity to stabilize a larger CO_2-insoluble core.

Table 2. The effect of CO_2 density on the self-assembly of PS-*b*-PFOA surfactants of varying block lengths.

Surfactant*	CO_2 density (g cm^{-3})†	N_{agg}	R_{core} (Å)	R_{total} (Å)	N_{CO_2}	Z_{core}
3.7^k-*b*-39.8^k	0.934	3.3	21	68	16	4.5
3.7^k-*b*-39.8^k	0.842	7	27	89	16	8
4.5^k-*b*-24.5^k	0.934	5	26	67	21	3
4.5^k-*b*-24.5^k	0.842	8	30	75	16	3
6.6^k-*b*-34.9^k	0.934	16	43	128	28	9
6.6^k-*b*-34.9^k	0.842	22	49	142	22	11
3.7^k-*b*-61.2^k	0.934	6	25	97	18	9
3.7^k-*b*-61.2^k	0.842	6	26	100	17	8

*Surfactant concentration = 4.0% (w/v). †Value for pure CO_2 at the temperature and pressure of the experiment (*32*).

Table 3. Effect of CO_2 density on the swelling of PS-*b*-PFOA surfactant micelles with a PS oligomer.

Surfactant*	[Oligomer]†	CO_2 density (g cm^{-3})‡	N_{agg}	R_{core} (Å)	R_{total} (Å)	N_{CO_2}	Z_{core}
3.7^k-*b*-39.8^k	13	0.934	10	44	124	13	11
3.7^k-*b*-39.8^k	13	0.842	12	47	120	7	11
3.7^k-*b*-39.8^k	16.6	0.934	11	48	126	9	12
3.7^k-*b*-39.8^k	16.6	0.842	13	50	119	5	11
4.5^k-*b*-24.5^k	20	0.934	40	70	157	10	10
4.5^k-*b*-24.5^k	20	0.842	39	69	152	7	8
6.6^k-*b*-34.9^k	20	0.934	20	64	153	15	9
6.6^k-*b*-34.9^k	20	0.842	22	66	162	11	10

*Surfactant concentration = 4.0% (w/v). †Oligomer concentration = percent (w/w) of surfactant; all experiments were performed with D-oligomer. ‡Value for pure CO_2 at the temperature and pressure of the experiment (*32*).

REFERENCES AND NOTES

1. K. A. Walsh, *Chem. Week* **158**, 38 (1996).
2. M. A. McHugh and V. J. Krukonis, *Supercritical Fluids Extraction: Principles and Practice* (Butterworth-Heinman, Stoneham, MA, ed. 2, 1993).
3. K. A. Shaffer and J. M. DeSimone, *Trends Polym. Sci.* **3**, 146 (1995).
4. J. A. Hyatt, *J. Org. Chem.* **49**, 5097 (1984).
5. V. S. Smith, P. O. Campbell, V. Vandana, A. S. Teja, *Int. J. Thermophys.* **1**, 23 (1996).
6. Z. Tuzar and P. Kratochiv, in *Surface and Colloid Science*, E. Matijevic, Ed. (Plenum, New York, 1993), vol. 15, pp. 1–83.
7. B. Chu, *Langmuir* **11**, 414 (1995).
8. J. C. Ravey, M. Buzier, C. Picot, *J. Colloid Interface Sci.* **97**, 9 (1984).
9. K. A. Cogan and A. P. Gast, *Macromolecules* **23**, 745 (1990).
10. J. L. Fulton *et al.*, *Langmuir* **11**, 4241 (1995).
11. K. P. Johnston *et al.*, *Science* **271**, 624 (1996).
12. K. A. Bartscherer, M. Minier, H. Renon, *Fluid Phase Equilibria* **107**, 93 (1995).
13. D. Chillura-Martin *et al.*, *J. Mol. Struct.*, in press.
14. J. Eastoe, Z. Bayazit, S. Martel, *Langmuir* **12**, 1423 (1996).
15. T. A. Hoefling, R. M. Enick, E. J. Beckman, *J. Phys. Chem.* **95**, 7127 (1991); E. J. Beckman, *Science* **271**, 613 (1996).
16. J. B. McClain *et al.*, *J. Am. Chem. Soc.* **118**, 917 (1996).
17. J. M. DeSimone, Z. Guan, C. S. Elsbernd, *Science* **257**, 945 (1992).
18. T. Otsu and M. Yoshida, *Makromol. Chem. Rapid Commun.* **3**, 127 (1982).
19. Z. Guan and J. M. DeSimone, *Macromolecules* **27**, 5527 (1994).
20. Summary of data from the synthesis of PS-*b*-PFOA diblock copolymers: Telechelic PS: $\langle M_n \rangle = 3.7$ kg mol^{-1}, polydispersity index (PDI) = 1.6, functionality = 1.6; 3.7^k-*b*-16.6^k diblock copolymer: $\langle M_n \rangle =$

20.4 kg mol^{-1}, 49.4 mol % styrene, and 50.6 mol % FOA; 3.7^{k}-*b*-39.8^{k} diblock copolymer: $\langle M_n \rangle$ = 43.5 kg mol^{-1}, 28.9 mol % styrene, and 71.1 mol % FOA; 3.7^{k}-*b*-61.2^{k} diblock copolymer: $\langle M_n \rangle$ = 64.9 kg mol^{-1}, 20.9 mol % styrene, and 79.1 mol % FOA. Telechelic PS: $\langle M_n \rangle$ = 4.5 kg mol^{-1}, PDI = 1.7, functionality = 1.6; 4.5^{k}-*b*-24.5^{k} diblock copolymer: $\langle M_n \rangle$ = 28.9 kg mol^{-1}, 44.5 mol % styrene, and 55.5 mol % FOA. Telechelic PS: $\langle M_n \rangle$ = 6.6 kg mol^{-1}, PDI = 1.8, functionality = 2.3; 4.5^{k}-*b*-34.9^{k} diblock copolymer: $\langle M_n \rangle$ = 41.5 kg mol^{-1}, 45.1 mol % styrene, and 54.9 mol % FOA.
21. L. J. Magid, *Colloid Surf. Sci.* **19**, 129 (1986).
22. W. C. Koehler, *Physica (Utrecht) B* **137**, 320 (1986).
23. R. J. Nelmes *et al*., *Acta Crystallogr.* **A49**, 427 (1993).
24. S. Janssen, D. Schwahn, K. Mortensen, T. Springer, *Macromolecules* **26**, 5587 (1993).
25. G. D. Wignall, in *The Physical Properties of Polymers*, J. E. Mark, Ed. (American Chemical Society, Washington, DC, 1993), pp. 313–378.
26. _____ and F. S. Bates, *J. Appl. Crystallogr.* **20**, 28 (1986).
27. Experiments were performed under equilibrium conditions, justified by an approximately 1-hour delay between the mixing of the system and the taking of data and by the observation that there was no change in the scattering curve during 3 to 8 hours of data acquisition.
28. E. Caponetti and R. Triolo, *Adv. Colloid Interface Sci.* **32**, 235 (1990); see also R. Triolo and E. Caponetti, in *Industrial and Technical Applications of Neutrons*, F. Rustichelli, M. Fontana, R. Coppola, Eds. (North-Holland, Amsterdam, 1992), pp. 403–424.
29. A. Halperin, M. Tirrell, T. P. Lodge, *Adv. Polym. Sci.* **100**, 31 (1992).
30. T. M. Birshtein and E. B. Zhulina, *Polymer* **30**, 171 (1989).
31. Y. Hsiao *et al*., *Macromolecules* **28**, 8159 (1995).
32. J. F. Ely, *CO_2PAC: A Computer Program to Calculate Physical Properties of Pure CO_2* (National Bureau of Standards, Boulder, CO, 1986).
33. The model CO_2-insoluble oligomers were PS (500 g mol^{-1}) made by living anionic polymerization. Also, to simplify the experimental system and to ensure minimal free oligomer dissolved in CO_2 under the experimental conditions, we extracted oligomer samples in advance with CO_2 at 50°C and 400 bar.
34. The research at the University of North Carolina was supported by the Environmentally Benign Chemical Synthesis and Processing Initiative of NSF and the U.S. Environmental Protection Agency; the Presidential Faculty Fellowship Program (J.M.D.); and the Consortium for the Synthesis and Processing of Polymeric Materials at the University of North Carolina (sponsored by Air Products and Chemicals, Bayer, B. F. Goodrich, DuPont, Eastman Chemical, General Electric, Hoechst-Celanese, and Xerox). The research at Oak Ridge National Laboratory was supported by Laboratory Directed Research and Development Program and the Division of Material Science, U.S. Department of Energy, under contract DE-AC05-96OR22464 with Lockheed Martin Energy Research Corp.

12 June 1996; accepted 25 September 1996

Grain Growth Rates of $MgSiO_3$ Perovskite and Periclase Under Lower Mantle Conditions

Daisuke Yamazaki,* Takumi Kato, Eiji Ohtani, Mitsuhiro Toriumi

The grain growth rates of $MgSiO_3$ perovskite and periclase in aggregates have been determined at 25 gigapascals and 1573 to 2173 kelvin. The average grain size (G) was fitted to the rate equation, and the grain growth rates of perovskite and periclase were $G^{10.6} = 1 \times 10^{-57.4}\ t \exp(-320.8/RT)$ and $G^{10.8} = 1 \times 10^{-62.3}\ t \exp(-247.0/RT)$, respectively, where t is the time, R is the gas constant, and T is the absolute temperature. These growth rates provide insight into the mechanism for grain growth in minerals relevant to the Earth's lower mantle that will ultimately help define the rheology of the lower mantle.

Mantle dynamics depends on the rheology of the constituent materials and the transition from spinel, $(Mg,Fe)_2SiO_4$, to perovskite, $(Mg,Fe)SiO_3$, plus magnesiowustite, (Mg,Fe)O, that is believed to be responsible for the 660 km discontinuity, which separates the upper and lower mantle (*1*). Some tomographic studies suggest that high-velocity anomalies may correspond to a cold, subducted slab penetrating into the lower mantle (*2*). Grain growth rates and the intergranular texture of perovskite plus magnesiowustite are important factors for understanding the rheology of the lower mantle, because grain size and orientation should affect flow dynamics (*3*). Karato *et al.* (*3*) suggested that the dominant deformation mechanism in perovskite is volume diffusion creep at lower mantle conditions when the average grain size is less than 1 mm. In this case, the effective viscosity is proportional to the square of the grain size. The evidence for a lack of seismic anisotropy in the lower mantle is consistent with deformation by diffusion creep (*4*). However, grain growth rates of lower mantle minerals have not been determined, and direct experimental determination of the rate laws is needed.

We conducted annealing experiments at pressures up to 25 GPa to determine the grain growth rates of aggregates of perovskite ($MgSiO_3$) and periclase (MgO), using a multianvil apparatus (*5*). A fine powder (<1-μm grain size) of synthetic forsterite was loaded in the apparatus at room temperature and the pressure was increased to 25 GPa, which corresponds to about 700 km depth in the mantle (*6*). Then the sample was heated at a constant rate of 100°C per minute to the run temperature which ranged from 1573 to 2173 K (*7*). Run durations at constant temperature ranged from a few seconds to 1897 min (*8*). The run products were investigated using a scanning electron microscope (SEM) to measure grain sizes, an electron microprobe to determine the composition of each phase, and an x-ray diffractometer to determine the structure of each phase. The grain boundaries were traced on backscattered electron images (BSE) of thin sections, using computerized image-processing. The grain sizes were estimated from the area of each grain, assuming the irregular grain boundary outlines could be approximated by a circle. Schwartz-Saltykovs method (*9*) was used to estimate the three-dimensional average grain size from the estimated grain areas (Table 1).

At low temperature (1573 K) and short duration (6 min), aggregates of perovskite and periclase formed eutectoid-like grains with equigranular spinel grains (Fig. 1A) (*10*). The eutectoid texture may be due to the growth of nuclei, controlled by atomic diffusion toward the interface between the host grain that contains the nuclei and the high-pressure phases already created in the

Table 1. Experimental conditions and calculated average grain size (*9*) for perovskite (Pv) and periclase (Pc). For each experiment, the forsterite (Fo) powder was held at 25 GPa at constant temperature (T) for the given duration. The Fo was transformed to a mixture of equigranular Pv and Pc in all the runs except PV13 (only equigranular spinel was observed) and PV20 (spinel, perovskite, and periclase were observed in a eutectoid texture). Numbers in parentheses are the standard deviations (1σ) for the grain size distributions; f.s., run duration is a few seconds (*8*); n.d., not determined because the grain size was less than 0.5 μm and could not be measured.

Run no.	T (K)	Duration (min)	Grain size	
			Pv (μm)	Pc (μm)
PV13	1573	f.s.	n.d.	n.d.
PV20	1573	6	n.d.	n.d.
PV10	1573	60	0.75 (0.26)	n.d.
PV17	1573	600	0.92 (0.26)	0.67 (0.16)
PV15	1873	f.s.	0.88 (0.22)	0.67 (0.17)
PV22	1873	19	1.03 (0.28)	0.80 (0.18)
PV11	1873	60	1.29 (0.34)	1.07 (0.24)
PV21	1873	190	1.27 (0.38)	1.03 (0.26)
PV18	1873	600	1.30 (0.36)	1.07 (0.30)
PV23	1873	1897	1.69 (0.46)	1.15 (0.33)
PV16	2173	f.s.	1.10 (0.31)	0.82 (0.22)
PV12	2173	60	1.61 (0.43)	1.12 (0.29)
PV19	2173	600	1.72 (0.48)	1.29 (0.36)

D. Yamazaki and M. Toriumi, Geological Institute, Faculty of Science, University of Tokyo, Bunkyo, Tokyo 113, Japan.
T. Kato, Institute of Geoscience, University of Tsukuba, Tsukuba, Ibaragi 305, Japan.
E. Ohtani, Institute of Mineralogy, Petrology and Economic Geology, Tohoku University, Sendai 980-77, Japan.

*To whom corresponce should be addressed. E-mail: daisuke@geol.s.u-tokyo.ac.jp